Hopf bifurcation and phase synchronization in memristor-coupled Hindmarsh–Rose and FitzHugh–Nagumo neurons with two time delays

Zhan-Hong Guo(郭展宏), Zhi-Jun Li(李志军)†, Meng-Jiao Wang(王梦蛟), and Ming-Lin Ma(马铭磷)

School of Automation and Electronic Information,Xiangtan University, Xiangtan 41110, *China*

(Received 2 September 2022; revised manuscript received 24 October 2022; accepted manuscript online 25 November 2022)

A memristor-coupled heterogenous neural network consisting of two-dimensional (2D) FitzHugh–Nagumo (FHN) and Hindmarsh–Rose (HR) neurons with two time delays is established. Taking the time delays as the control parameters, the existence of Hopf bifurcation near the stable equilibrium point in four cases is derived theoretically, and the validity of the Hopf bifurcation condition is verified by numerical analysis. The results show that the two time delays can make the stable equilibrium point unstable, thus leading to periodic oscillations induced by Hopf bifurcation. Furthermore, the time delays in FHN and HR neurons have different effects on the firing activity of neural network. Complex firing patterns, such as quiescent state, chaotic spiking, and periodic spiking can be induced by the time delay in FHN neuron, while the neural network only exhibits quiescent state and periodic spiking with the change of the time delay in HR neuron. Especially, phase synchronization between the heterogeneous neurons is explored, and the results show that the time delay in HR neurons has a greater effect on blocking the synchronization than the time delay in FHN neuron. Finally, the theoretical analysis is verified by circuit simulations.

Keywords: memristor, time delay, heterogeneous neurons, hopf bifurcation, phase synchronization

PACS: 87.19.ll, 87.19.lj, 05.45.Pq **DOI:** 10.1088/1674-1056/aca601

1. Introduction

Neurons, as basic structural and functional units of the nervous systems, have the functions of sensing stimuli and generating action potential. The firing pattern of neurons plays a vital role in coding and processing of neuronal signals. To theoretically discover the complex firing activities of biological neurons, many simplified models have been derived from the classical four-dimensional Hodgkin–Huxley (HH) model, such as FitzHugh–Nagumo (FHN),[1–3] Hindmarsh–Rose (HR),[4,5] Morris–Lecar (ML),[6,7] and Rulkov.[8] Based on these simplified models, some novel theoretical results have been acquired.[9–19] For example, an adaptive method was proposed to modulate the output of FHN neuron.[10] Complex firing patterns of HR neuron induced by electromagnetic induction were revealed in Refs. [11,12]. Three types of firing patterns induced by one parameter were revealed in a modified ML neuron.[13] Other studies which discussed the firing patterns of neurons can be found in Refs. [14–19].

Since Chua first proposed the concept of memristor,[20] it has created considerable research interest.[21–24] In biology, synapses are key structures for information transmission between neurons.[25] Memristor is considered as an ideal physical device to simulate neuronal synapses due to its unique characteristics, *i.e.*, nanoscale, memorability, and nonlinearity.[26,27] To investigate the collective firing activities of neurons, considering memristors as synapses to bridge neurons has attracted extensive attention in the community of scholars. A neural model constructed with two 2D HR neurons and a locally-active memristive autapse was established and the authors found that the complicated firing behaviors only occur within the locally active region of the memristor.[28] By utilizing a multi-stable memristor as a coupling synapse, Lin and Wang[29] established a memristive Hopfield neural network, which can exhibit infinitely many coexisting chaotic attractors under different initial conditions. More interesting, counterintuitive firing behaviors were also found in memristor-based neural networks. For example, the decrease of firing rates induced by increasing excitatory memristive synaptic current, and the increase of firing rates induced by increasing inhibitory memristive synaptic current were revealed in memristor-based HR neuron.[30] Furthermore, periodic bursting and multi-scroll chaotic bursting were also explored in a neural system with memristive synapse.[31] Synchronization between neurons is critical for learning and memory formation, thus, it is significant and necessary to study the synchronization between homogeneous and heterogeneous neurons. Xu *et al.* constructed a five-dimensional neural network by utilizing a memristor to connect two FHN neurons.[32] They found synchronization can be enhanced under memristor coupling and appropriate noise is also helpful for synchronization stability. The exponential synchronization in the memristor-coupled two three-dimensional (3D) HR neurons was proved by Bao *et al.*[33] Employing a memristor to couple two heterogeneous neurons, Li *et al.* found that two nonidentical neurons gradually become phase synchronized with the increase of the

†Corresponding author. E-mail: lizhijun_320@163.com

© 2023 Chinese Physical Society and IOP Publishing Ltd

coupling strength.[34]

Due to the finite transmission speed of neural signals and the finite processing time in synapses, time delays are ubiquitous in biological neural systems. Numerous research results show that the time delay plays an important role in determining the firing activity of neurons. For isolated neurons, time delay can induce neuron to transition from quiescent regime to periodic oscillations ignited by Hopf bifurcation.[35] Furthermore, time delay can not only lead to complex bifurcation scenarios,[36] but also regulate effectively the firing frequency of neurons.[37] Other similar studies on single neurons with time delay can be found in Refs. [38–40]. While for neural network constructed with multiple neurons, time delay plays a subtle role in either promoting or impeding synchronization.[41–44] Huang *et al.* found that the desynchronization of firing in a neural system is increasingly enhanced with the increase of time delay.[45] A linearly coupled memristorbased recurrent neural network with impulses and time-varying delay was proposed, and the sufficient conditions of exponential synchronization were derived in Ref. [46]. In a pair of coupled FitzHugh–Nagumo neurons, multiple transitions between in-phase and anti-phase synchronizations induced by the time delay were simulated for the inhibitory and excitatory couplings.[47]

From the above studies, one can find that, on one hand, considering memristor as a coupling synapse in the neural system is an effective method to study complex firing activities of biological neural systems, on the other hand, time delay can not only cause the transition of firing patterns, but also affect the synchronous behavior of neurons. However, the effect of time delay on the firing activities is rarely considered in the existing memristor-coupled neural systems. Furthermore, most memristor-coupled neural systems are constructed with the same neurons or non-identical neurons governed by the same mathematical model. In fact, from sensing external stimuli to generating corresponding action potentials, neural system needs the cooperation of different neurons distributed in different functional areas. Therefore, studying the synchronous behavior of different neurons is of great value for understanding the operating mechanism of the nervous system.

In order to further explore the effects of multiple time delays on the collective firing activities of the memristor-coupled neural system, a novel neural network constructed with 2D FHN neuron and HR neuron coupled by a memristive synapse is established in this study, where the time delays in FHN neuron and HR neuron are all considered. The stability of the equilibrium points and the existence of the local Hopf bifurcation are analyzed in four cases, and the numerical analysis is performed to verify the effectiveness of the local Hopf bifurcation conditions. The effects of time delays on phase synchronization between two heterogeneous neurons are also discussed.

The paper is organized as follows. In Section 2, a neural system with memristive synapse coupling HR neuron and FHN neuron is established. The local stability of the equilibrium points and the existence of the local Hopf bifurcation are obtained in Section 3. The effect of time delays on phase synchronization is discussed in Section 4. In Section 5, neural network circuit is developed and circuit simulation results are provided. Conclusions are given in the last section.

2. Model description

2.1. Memristor model

Memristor as an ideal device for simulating neural synapse, its memductance function plays a crucial role in determining firing activities of memristor-based neural networks. To mimic the threshold effect of neuron, the hyperbolic tangent saturation function, is utilized to characterize the memductance function, and thus a novel threshold memristor model is proposed as[33]

$$i = w(\phi)v = [\alpha + \beta \tanh(\phi)]v, \tag{1}$$

$$\frac{\mathrm{d}\phi}{\mathrm{d}t} = g(\phi, v) = -\phi + 0.2v, \tag{2}$$

where v and i represent the input voltage and output current, $w(\phi)$ is memductance and ϕ is the internal state variable, α and β are memristive parameters.

2.2. Memristor synapse-coupled neuron model

The firing activities of a single 2D HR neuron or FHN neuron are simple, but complex firing phenomena emerge when they are coupled together.[34] Besides, time delay is ubiquitous in the neural systems due to the limited transmission speed of neural signals. As a non-negligible factor, the effect of time delay is considered in this study. Based on the 2D FHN and HR neurons, a novel neural network with two time delays is developed and written as

$$\begin{cases} \dfrac{\mathrm{d}x_1}{\mathrm{d}t} = x_1 - \dfrac{1}{3}x_1^3 - y_1 - k[\alpha + \beta\tanh\phi] \\ \qquad \times [x_1(t-\tau_1) - x_2(t-\tau_2)], \\ \dfrac{\mathrm{d}y_1}{\mathrm{d}t} = e(x_1 + a_1 - b_1 y_1), \\ \dfrac{\mathrm{d}x_2}{\mathrm{d}t} = y_2 - a_2 x_2^3 + b_2 x_2^2 + k[\alpha + \beta\tanh\phi] \\ \qquad \times [x_1(t-\tau_1) - x_2(t-\tau_2)], \\ \dfrac{\mathrm{d}y_2}{\mathrm{d}t} = c - d x_2^2 - y_2, \\ \dfrac{\mathrm{d}\phi}{\mathrm{d}t} = -\phi + 0.2[x_1(t-\tau_1) - x_2(t-\tau_2)], \end{cases} \tag{3}$$

where the first two formulas represent the 2D FHN neuron, whose parameters are set as the classical values of $a_1 = 0.6$, $b_1 = 0.5$, and $e = 0.1$;[40] the third and fourth formulas denote the 2D HR neuron, its classical parameters are determined as

$a_2 = 1$, $b_2 = 3$, $c = 1$, and $d = 5$;[34] the last one is the internal state equation of the threshold memristor, α and β are the memristor's parameters which are selected as $\alpha = 0.5$ and $\beta = 1$; τ_1 and τ_2 are the time delays of signal transmission in FHN neuron and HR neuron, respectively, and k is the coupling strength.

3. Stability of equilibrium and Hopf bifurcation analysis

3.1. Stability of equilibrium

In this section, we mainly investigate the conditions of the local Hopf bifurcation in four different cases based on the characteristic equation of the proposed system. When $\tau_1 = \tau_2 = 0$, system (3) turns into a non-delay system. Let the left side of system (3) equal 0, the corresponding equilibrium point can be represented as $E(x_1, 2x_1 + 1.2, x_2, 1-5x_2^2, 0.2(x_1 - x_2))$, where the values of x_1 and x_2 corresponding to the intersections of two following functions:

$$\begin{aligned} f_1(x_1,x_2) &= -x_1^3/3 - x_1 - 1.2 \\ &\quad - k\{0.5 + \tanh[0.2(x_1 - x_2)]\}(x_1 - x_2), \quad (4) \\ f_2(x_1,x_2) &= 1 - 2x_2^2 - x_2^3 \\ &\quad + k\{0.5 + \tanh[0.2(x_1 - x_2)]\}(x_1 - x_2), \quad (5) \end{aligned}$$

By means of graphic analytic method, the curves of $f_1(x_1, x_2)$ and $f_2(x_1, x_2)$ with $k = 1$ are illustrated in Fig. 1. Observe that there exist three equilibrium points. The eigenvalues and stabilities corresponding to different equilibrium points are listed in Table 1. From Table 1, one can see that there is only one stable point E_1, and the other two points E_2 and E_3 are unstable. The time series of membrane potentials of FHN and HR neurons are shown in Figs. 2(a), 2(b), and 2(c) when the initial values are close to E_1, E_2, and E_3 respectively. It is easy to find that when the initial value is fixed near the stable equilibrium point E_1, both neurons are quiescent. However, once the initial values are specified near the unstable equilibrium points E_2 and E_3, the two neurons exhibit different bursting oscillations, respectively. Since E_1 is the unique stable equilibrium point in system (3), this paper, thus, only discusses the local Hopf bifurcation of the stable equilibrium point E_1.

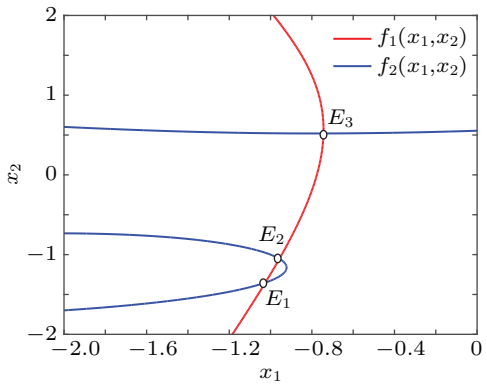


Fig. 1. The equilibrium points of system (3), which correspond to the intersections of the curves $f_1(x_1, x_2)$ and $f_2(x_1, x_2)$. The equilibrium point E_1 is a stable node, while the equilibrium points E_2 and E_3 are saddle-foci.

Table 1. Equilibrium points along with their corresponding eigenvalues and stabilities for $k = 1$.

No.	$(\bar{x}_1, \bar{x}_2)$	Eigenvalues	Stabilities
E_1	$(-1.0253, -1.3517)$	$-15.1303, -0.7477, -0.6595, -0.2101, -0.045$	stable node point
E_2	$(-0.9571, -1.0522)$	$-11.2074, -0.9703, 0.049, -0.255 \pm j0.206$	unstable saddle-focus
E_3	$(-0.7438, 0.5198)$	$-1.2061, 0.0916 \pm j0.25, 0.4423 \pm j1.6436$	unstable saddle-focus

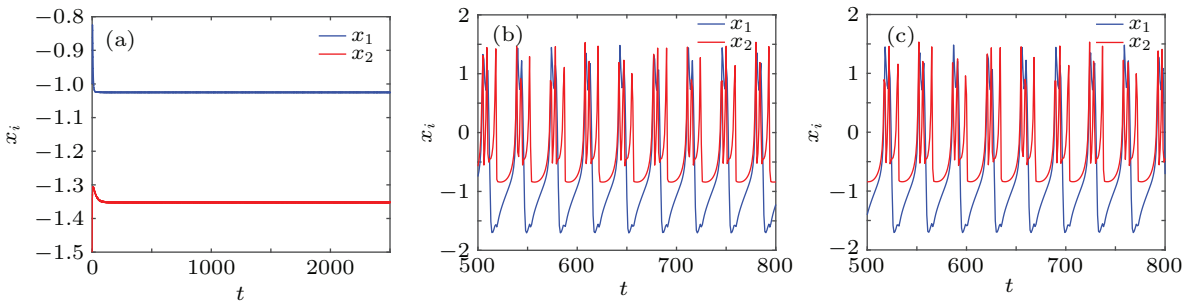


Fig. 2. The time series of membrane potentials of FHN and HR neurons with different initial values: (a) $x_1 = -1$, $y_1 = -1$, $x_2 = -1.5$, $y_2 = -8$, $\phi = 0$; (b) $x_1 = -1$, $y_1 = -0.7$, $x_2 = -1$, $y_2 = -4.5$, $\phi = 0$; (c) $x_1 = -0.7$, $y_1 = -0.3$, $x_2 = 0.5$, $y_2 = -0.3$, $\phi = 0$. The coupling strength $k = 1$, x_1 and x_2 denote the membrane potentials of FHN and HR neurons, respectively.

3.2. Hopf bifurcation analysis

In general, neurons are excitable because they are near bifurcations from resting to spiking activity. Hopf bifurcation can induce the transition from resting to periodic spiking behavior in neurons.[48] Considering the fact that the neural system (3) has only one stable equilibrium point, so, we mainly focus on the existence of local Hopf bifurcation of the stable equilibrium point E_1.

By linearizing system (3) at equilibrium point E_1 with $k = 1$, the corresponding Jacobian matrix[49] is obtained as

$$J_{E_1}=\begin{bmatrix} 1-\bar{x}_1^2-\left[0.5+\tanh\bar{\phi}\right]\mathrm{e}^{-\lambda\tau_1} & -1 & \left[0.5+\tanh\bar{\phi}\right]\mathrm{e}^{-\lambda\tau_2} & 0 & -\operatorname{sech}^2\bar{\phi}(\bar{x}_1-\bar{x}_2) \\ 0.1 & -0.05 & 0 & 0 & 0 \\ \left[0.5+\tanh\bar{\phi}\right]\mathrm{e}^{-\lambda\tau_1} & 0 & -3\bar{x}_2^2+6\bar{x}_2-\left[0.5+\tanh\bar{\phi}\right]\mathrm{e}^{-\lambda\tau_2} & 1 & \operatorname{sech}^2\bar{\phi}(\bar{x}_1-\bar{x}_2) \\ 0 & 0 & -10\bar{x}_2 & -1 & 0 \\ 0.2\mathrm{e}^{-\lambda\tau_1} & 0 & -0.2\mathrm{e}^{-\lambda\tau_2} & 0 & -1 \end{bmatrix}$$

and the corresponding characteristic equation can be written as

$$\lambda^5+B_1\lambda^4+B_2\lambda^3+B_3\lambda^2+B_4\lambda+B_5+H_1(\lambda)\mathrm{e}^{-\lambda\tau_1}+H_2(\lambda)\mathrm{e}^{-\lambda\tau_2}=0, \tag{6}$$

where

$$\begin{aligned} B_1&=1.05-6\bar{x}_2+\bar{x}_1^2+3\bar{x}_2^2,\\ B_2&=-0.85+3.7\bar{x}_2+2.05\bar{x}_1^2+3.15\bar{x}_2^2-6\bar{x}_1^2\bar{x}_2+3\bar{x}_1^2\bar{x}_2^2,\\ B_3&=-0.85+5.6\bar{x}_2+1.1\bar{x}_1^2-2.55\bar{x}_2^2-2.3\bar{x}_1^2\bar{x}_2+6.15\bar{x}_1^2\bar{x}_2^2,\\ B_4&=0.05-3.9\bar{x}_2+0.05\bar{x}_1^2-2.55\bar{x}_2^2+3.9\bar{x}_1^2\bar{x}_2+3.3\bar{x}_1^2\bar{x}_2^2,\\ B_5&=0.2\bar{x}_2+0.15\bar{x}_2^2+0.2\bar{x}_1^2\bar{x}_2+0.15\bar{x}_1^2\bar{x}_2^2,\\ H_1(\lambda)&=C_1\lambda^4+C_2\lambda^3+C_3\lambda^2+C_4\lambda+C_5,\\ H_2(\lambda)&=D_1\lambda^4+D_2\lambda^3+D_3\lambda^2+D_4\lambda+D_5, \end{aligned} \tag{7}$$

with

$$\begin{aligned} C_1&=0.5+\tanh\bar{\phi},\\ C_2&=1.025+\frac{0.2(\bar{x}_1-\bar{x}_2)}{\cosh^2\bar{\phi}}-3\bar{x}_2+1.5\bar{x}_2^2+2.05\tanh\bar{\phi}-6\bar{x}_2\tanh\bar{\phi}+3\bar{x}_2^2\tanh\bar{\phi},\\ C_3&=\frac{(1.2\bar{x}_2^2-0.6\bar{x}_2^3+0.21\bar{x}_1-0.21\bar{x}_2-1.2\bar{x}_1\bar{x}_2+0.6\bar{x}_1\bar{x}_2^2)}{\cosh^2\bar{\phi}}+0.55-1.15\bar{x}_2+3.075\bar{x}_2^2\\ &\quad+1.1\tanh\bar{\phi}-2.3\bar{x}_2\tanh\bar{\phi}+6.15\bar{x}_2^2\tanh\bar{\phi},\\ C_4&=\frac{(0.01\bar{x}_1-0.74\bar{x}_2^2-0.63\bar{x}_2^3-0.01\bar{x}_2+0.74\bar{x}_1\bar{x}_2+0.63\bar{x}_1\bar{x}_2^2)}{\cosh^2\bar{\phi}}+0.025+1.95\bar{x}_2\\ &\quad+1.65\bar{x}_2^2+0.05\tanh\bar{\phi}+3.9\bar{x}_2\tanh\bar{\phi}+3.3\bar{x}_2^2\tanh\bar{\phi},\\ C_5&=\frac{(-0.04\bar{x}_2^2-0.03\bar{x}_2^3+0.04\bar{x}_1\bar{x}_2+0.03\bar{x}_1\bar{x}_2^2)}{\cosh^2\bar{\phi}}+0.1\bar{x}_2+0.075\bar{x}_2^2+0.2\bar{x}_2\tanh\bar{\phi}+0.15\bar{x}_2^2\tanh\bar{\phi},\\ D_1&=0.5+\tanh\bar{\phi},\\ D_2&=\frac{(0.2\bar{x}_1-0.2\bar{x}_2)}{\cosh^2\bar{\phi}}+0.525+0.5\bar{x}_1^2+1.05\tanh\bar{\phi}+\bar{x}_1^2\tanh\bar{\phi},\\ D_3&=\frac{(0.2\bar{x}_1^3+0.01\bar{x}_1-0.01\bar{x}_2-0.2\bar{x}_1^2\bar{x}_2)}{\cosh^2\bar{\phi}}-0.425+1.025\bar{x}_1^2-0.85\tanh\bar{\phi}+2.05\bar{x}_1^2\tanh\bar{\phi},\\ D_4&=\frac{(0.21\bar{x}_1^3-0.18\bar{x}_1+0.18\bar{x}_2-0.21\bar{x}_1^2\bar{x}_2)}{\cosh^2\bar{\phi}}-0.425+0.55\bar{x}_1^2-0.85\tanh\bar{\phi}+1.1\bar{x}_1^2\tanh\bar{\phi},\\ D_5&=\frac{(0.01\bar{x}_1^3+0.01\bar{x}_1-0.01\bar{x}_2-0.01\bar{x}_1^2\bar{x}_2)}{\cosh^2\bar{\phi}}+0.025+0.025\bar{x}_1^2+0.05\tanh\bar{\phi}+0.05\bar{x}_1^2\tanh\bar{\phi}. \end{aligned}$$

For different time delays τ_1 and τ_2, the existence of Hopf bifurcation in four cases is discussed, respectively.

Case 1 $\tau_1=0,\ \tau_2>0$. The characteristic equation (6) becomes

$$\lambda^5+(B_1+C_1)\lambda^4+(B_2+C_2)\lambda^3+(B_3+C_3)\lambda^2+(B_4+C_4)\lambda+B_5+C_5+H_2(\lambda)\mathrm{e}^{-\lambda\tau_2}=0. \tag{8}$$

If Hopf bifurcation exists, then $\lambda=\mathrm{i}\omega(\omega>0)$ is a root of Eq. (8). Substituting $\lambda=\mathrm{i}\omega$ into Eq. (8), one can get

$$\begin{aligned} &\mathrm{i}\omega^5+(B_1+C_1)\omega^4-(B_2+C_2)\omega^3\mathrm{i}-(B_3+C_3)\omega^2+(B_4+C_4)\omega\mathrm{i}+(B_5+C_5)+(D_1\omega^4\\ &-D_2\omega^3\mathrm{i}-D_3\omega^2+D_4\omega\mathrm{i}+D_5)\times[\cos(\omega\tau_2)-\mathrm{i}\sin(\omega\tau_2)]=0. \end{aligned} \tag{9}$$

Separating the real and imaginary parts of Eq. (9) obtains the following equations

$$\begin{cases} A_1+m\cos(\omega\tau_2)+n\sin(\omega\tau_2)=0,\\ A_2-m\sin(\omega\tau_2)+n\cos(\omega\tau_2)=0, \end{cases} \tag{10}$$

where

$$A_1=(B_1+C_1)\omega^4-(B_3+C_3)\omega^2+(B_5+C_5),$$

$$A_2 = \omega^5 - (B_2 + C_2)\omega^3 + (B_4 + C_4)\omega,$$
$$m = D_1\omega^4 - D_3\omega^2 + D_5,$$
$$n = D_4\omega - D_2\omega^3. \tag{11}$$

Using $\sin^2(\omega\tau_2) + \cos^2(\omega\tau_2) = 1$, we have the following expression:

$$\omega^{10} + e_1\omega^8 + e_2\omega^6 + e_3\omega^4 + e_4\omega^2 + e_5 = 0, \tag{12}$$

where

$$\begin{aligned}
e_1 &= (B_1 + C_1)^2 - 2(B_2 + C_2) - D_1^2,\\
e_2 &= (B_2 + C_2)^2 + 2(B_4 + C_4)\\
&\quad - 2(B_1 + C_1)(B_3 + C_3) + 2D_1D_3 - D_2^2,\\
e_3 &= (B_3 + C_3)^2 + 2(B_5 + C_5)(B_1 + C_1)\\
&\quad - 2(B_4 + C_4)(B_2 + C_2) - D_3^2 - 2D_1D_5 + 2D_2D_4,\\
e_4 &= (B_4 + C_4)^2 - 2(B_5 + C_5)(B_3 + C_3) + 2D_3D_5 - D_4^2,\\
e_5 &= (B_5 + C_5)^2 - D_5^2.
\end{aligned}$$

By substituting the stable equilibrium point E_1 into Eq. (12), and the unique positive real root $\omega = 0.032068$ is obtained by using Matlab. At the same time, the expression of time delay τ_2 about ω can be gained by sorting Eq. (10) as follows:

$$\tau_2^{(j)} = \frac{1}{\omega}\left\{\arcsin\frac{A_2m - A_1n}{m^2 + n^2} + 2j\pi\right\}, \tag{13}$$

where j is a natural number, solving Eq. (13), we get $\tau_2^{(j)} = 47.287 + 195.9j$.

Define $\tau_2^0 = 47.287$ as the Hopf bifurcation point. When τ_2 is less than or greater than the critical value τ_2^0, the time series of membrane potentials of FHN and HR neurons are shown in Figs. 3 and 4, respectively. The inter-spike intervals (ISI) bifurcation diagram of membrane potential x_1 with respect to τ_2 is illustrated in Fig. 5. When $\tau_1 = 0$ and $\tau_2 < \tau_2^0 = 47.287$, both neurons are in a quiescent state first. Once τ_2 surpasses the critical value $\tau_2^0 = 47.287$, FHN and HR neurons suddenly exhibit periodic firing due to the effect of the local Hopf bifurcation.

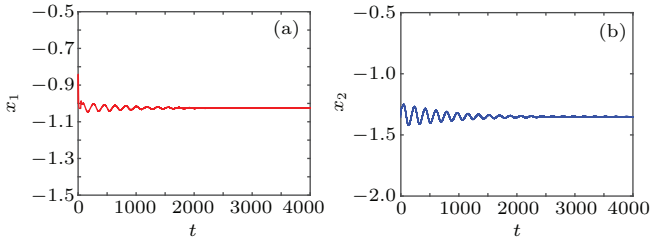


Fig. 3. The time series of membrane potentials. (a) FHN neuron, (b) HR neuron. The coupling strength $k = 1$, the initial value is fixed near the equilibrium point with ($x_1 = -1$, $y_1 = -1.01$, $x_2 = -1.36$, $y_2 = -8$, $\phi = 0.065$) and the time delay $\tau_2 = 46$. Since the time delay τ_2 is less than the critical value 47.287, both neurons are quiescent.

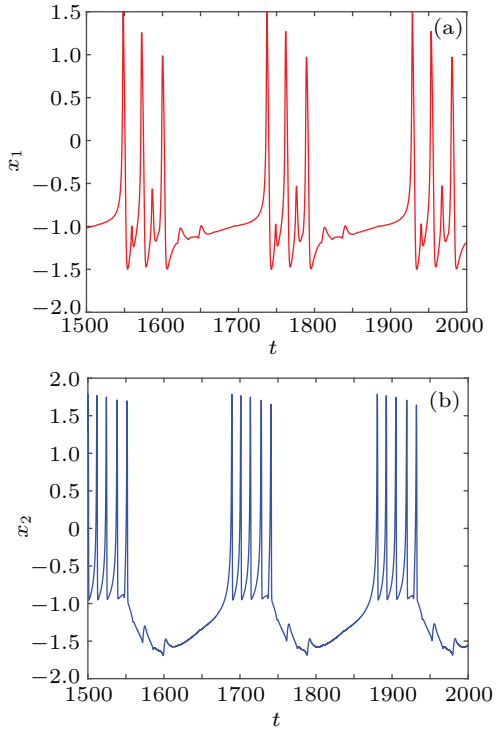


Fig. 4. The time series of membrane potentials. (a) FHN neuron, (b) HR neuron. The coupling strength $k = 1$, the initial value is ($x_1 = -1$, $y_1 = -1.01$, $x_2 = -1.36$, $y_2 = -8$, $\phi = 0.065$), and the time delay $\tau_2 = 47.5$. Periodic bursting emerges in two neurons due to the time delay $\tau_2 > \tau_2^0 = 47.287$.

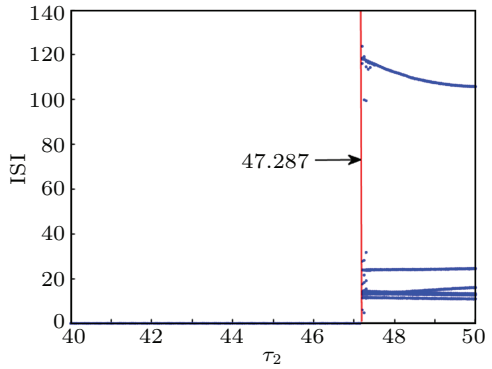


Fig. 5. ISI bifurcation diagram of membrane potential x_1 with respect to the time delay τ_2. The coupling strength $k = 1$, and the initial value is fixed near the ($x_1 = -1$, $y_1 = -1.01$, $x_2 = -1.36$, $y_2 = -8$, $\phi = 0.065$).

Case 2 $\tau_1 > 0$, $\tau_2 = 0$. The characteristic equation (6) becomes

$$\lambda^5 + (B_1 + D_1)\lambda^4 + (B_2 + D_2)\lambda^3 + (B_3 + D_3)\lambda^2 + (B_4 + D_4)\lambda + (B_5 + D_5) + H_1(\lambda)\mathrm{e}^{-\lambda\tau_1} = 0. \tag{14}$$

Substituting $\lambda = \mathrm{i}\omega$ into Eq. (14), separating the real and imaginary part, and using the same method as in Case 1, we can get

$$\omega^{10} + e_1\omega^8 + e_2\omega^6 + e_3\omega^4 + e_4\omega^2 + e_5 = 0, \tag{15}$$

where

$$e_1 = (B_1 + D_1)^2 - 2(B_2 + D_2) - C_1^2,$$

$$
\begin{aligned}
e_2 &= (B_2+D_2)^2+2(B_4+D_4)\\
&\quad -2(B_1+D_1)(B_3+D_3)+2C_1C_3-C_2^2,\\
e_3 &= (B_3+D_3)^2+2(B_5+D_5)(B_1+D_1)-2(B_4+D_4)\\
&\quad \times(B_2+D_2)-C_3^2-2C_1C_5+2C_2C_4,\\
e_4 &= (B_4+D_4)^2-2(B_5+D_5)(B_3+D_3)+2C_3C_5-C_4^2,\\
e_5 &= (B_5+D_5)^2-C_5^2. \qquad (16)
\end{aligned}
$$

Solving Eq. (15), we get $\omega_1 = 0.138664$ and $\omega_2 = 0.675954$, which correspond to $\tau_{11}^{(j)} = -9.47+45.3j$ and $\tau_{12}^{(j)} = 1.65+9.3j$, respectively. Since the time delay is a non-negative value, the Hopf bifurcation point can be derived as $\tau_1^0 = \min\limits_{n=1,2}\{\tau_{1n}^{(0)}\} = 1.65$. The time series of membrane potentials for FHN and HR neurons around bifurcation point are plotted in Fig. 6 and 7 respectively, the ISI bifurcation diagram of membrane potential x_1 is shown in Fig. 8.

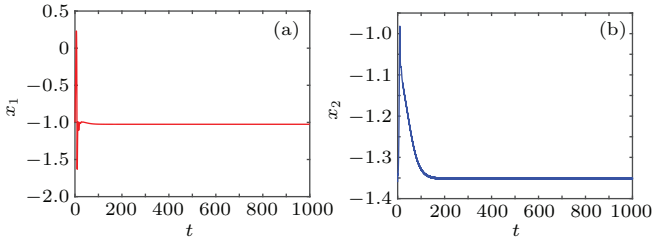


Fig. 6. The time series of membrane potentials. (a) FHN neuron, (b) HR neuron. The coupling strength $k = 1$, the initial value is $(x_1 = -1, y_1 = -1.05, x_2 = -1.36, y_2 = -8, \phi = 0.065)$. Two neurons are quiescent due to the time delay $\tau_1 = 1.6$, which is less than the critical value $\tau_1^0 = 1.65$.

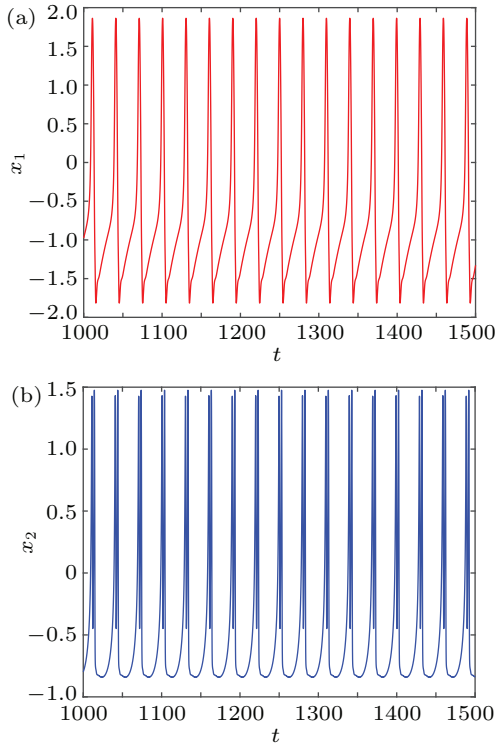


Fig. 7. The time series of membrane potentials. (a) FHN neuron, (b) HR neuron. The coupling strength $k = 1$, the initial value is $(x_1 = -1, y_1 = -1.05, x_2 = -1.36, y_2 = -8, \phi = 0.065)$. Periodic oscillations emerge in two neurons due to the time delay $\tau_1 = 1.7$, which is more than the critical value $\tau_1^0 = 1.65$.

From Fig. 8, we can find that with increase of τ_1, the FHN neuron transits from quiescent regime to periodic firing through Hopf bifurcation. The neuron shows chaotic spiking when τ_1 is between 2.55 and 4.47, and then a periodic window appears when $4.47 < \tau_1 < 4.6$. The time series of membrane potentials for both neurons with the time delay $\tau_1 = 4$ are shown in Figs. 9(a) and 9(b).

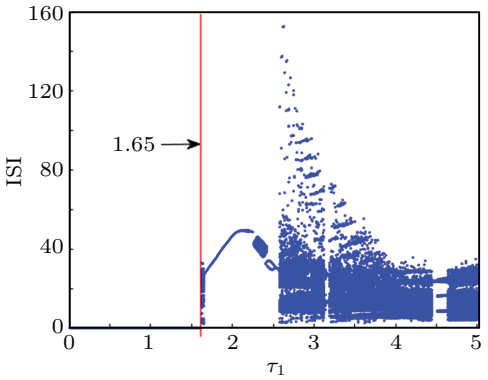


Fig. 8. ISI bifurcation diagram of membrane potential x_1 of FHN neuron with respect to the time delay τ_1. The coupling strength $k = 1$ and the initial value $(x_1 = -1, y_1 = -1.05, x_2 = -1.36, y_2 = -8, \phi = 0.065)$.

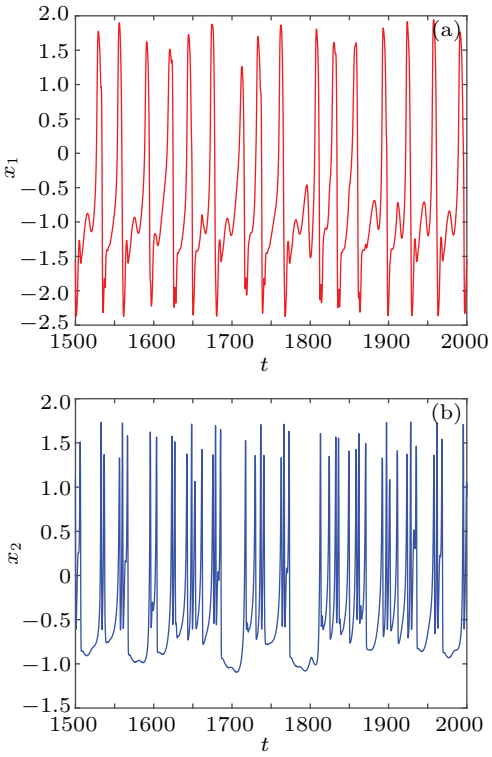


Fig. 9. The time series of membrane potentials. (a) FHN neuron, (b) HR neuron. The coupling strength $k = 1$, the initial value is $(x_1 = -1, y_1 = -1.05, x_2 = -1.36, y_2 = -8, \phi = 0.065)$, and the time delay $\tau_1 = 4$. Both neurons exhibit chaotic spiking.

Case 3 $\tau_1 = \tau_2 = \tau \neq 0$. The characteristic equation (6) becomes

$$
\begin{aligned}
&\lambda^5+B_1\lambda^4+B_2\lambda^3+B_3\lambda^2+B_4\lambda+B_5\\
&+[(C_1+D_1)\lambda^4+(C_2+D_2)\lambda^3+(C_3+D_3)\lambda^2\\
&+(C_4+D_4)\lambda+(C_5+D_5)]\,\mathrm{e}^{-\lambda\tau}=0. \qquad (17)
\end{aligned}
$$

$\lambda = \mathrm{i}\omega$ is the root of Eq. (17) if and only if ω satisfies the following equation when Hopf bifurcation occurs

$$\begin{aligned}&\mathrm{i}\omega^5 + B_1\omega^4 - B_2\omega^3\mathrm{i} - B_3\omega^2 + B_4\omega\mathrm{i} + B_5\\&+[(C_1+D_1)\omega^4 - (C_2+D_2)\omega^3\mathrm{i} - (C_3+D_3)\omega^2\\&+(C_4+D_4)\omega\mathrm{i} + (C_5+D_5)]\,[\cos(\omega\tau) - \mathrm{i}\sin(\omega\tau)] = 0. \quad (18)\end{aligned}$$

By separating the real and imaginary parts of the above equation, we can obtain

$$\begin{cases} A_1 + m\cos(\omega\tau) + n\sin(\omega\tau) = 0,\\ A_2 - m\sin(\omega\tau) + n\cos(\omega\tau) = 0, \end{cases} \quad (19)$$

where

$$\begin{aligned}A_1 &= B_1\omega^4 - B_3\omega^2 + B_5,\\A_2 &= \omega^5 - B_2\omega^3 + B_4\omega,\\m &= (C_1+D_1)\omega^4 - (C_3+D_3)\omega^2 + (C_5+D_5),\\n &= (C_4+D_4)\omega - (C_2+D_2)\omega^3. \end{aligned} \quad (20)$$

It follows that

$$\omega^{10} + e_1\omega^8 + e_2\omega^6 + e_3\omega^4 + e_4\omega^2 + e_5 = 0, \quad (21)$$

where

$$\begin{aligned}e_1 &= B_1^2 - 2B_2 - (C_1+D_1)^2,\\e_2 &= B_2^2 + 2B_4 - 2B_1B_3 + 2(C_1+D_1)(C_3+D_3) - (C_2+D_2)^2,\\e_3 &= B_3^2 + 2B_5B_1 - 2B_4B_2 - (C_3+D_3)^2 - 2(C_1+D_1)\\&\quad\times(C_5+D_5) + 2(C_2+D_2)(C_4+D_4),\\e_4 &= B_4^2 - 2B_5B_3 + 2(C_3+D_3)(C_5+D_5) - (C_4+D_4)^2,\\e_5 &= B_5^2 - (C_5+D_5)^2. \end{aligned} \quad (22)$$

Three roots $\omega_1 = 0.0387$, $\omega_2 = 0.15$, and $\omega_3 = 0.771537$ are obtained by calculating Eq. (21) at E_1, which correspond to $\tau_1^{(j)} = -40.59 + 215.6j$, $\tau_2^{(j)} = -6.9 + 41.88j$, and $\tau_3^{(j)} = 2.036 + 7.57j$. Similarly, we can get the Hopf bifurcation point $\tau^0 = \min n = 1,2,3,\ldots\{\tau_n^{(0)}\} = 2.036$. Figures 10 and 11 illustrate the firing patterns of two neurons near bifurcation point, and the ISI bifurcation diagram of membrane potential x_1 is shown in Fig. 12.

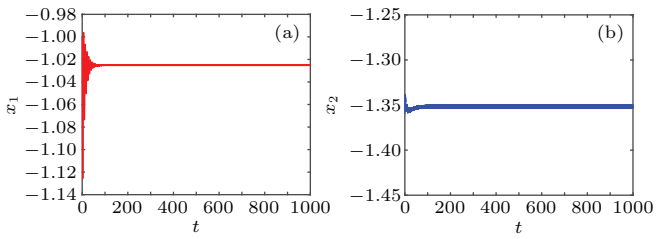


Fig. 10. The time series of membrane potentials. (a) FHN neuron, (b) HR neuron. The coupling strength $k = 1$, the initial value is ($x_1 = -1$, $y_1 = -0.8$, $x_2 = -1.36$, $y_2 = -8$, $\phi = 0.065$), and the time delays $\tau_1 = \tau_2 = 1.8$. Both neurons are quiescent due to the time delays are less than $\tau^0 = 2.036$.

It can be seen from Fig. 12 that the FHN neuron is quiescent when $0 < \tau < 2.036$. After the local Hopf bifurcation takes place at $\tau = 2.036$, it enters a short periodic state, and then transforms to chaotic state suddenly. When $3.5 < \tau < 5$, the ISI bifurcation diagram exhibits two lines, which means the neuron exhibits period-2 bursting oscillation. The time series of membrane potentials for FHN and HR neurons when $\tau = 2.5$ and 4 are shown in Figs. 13 and 14, respectively.

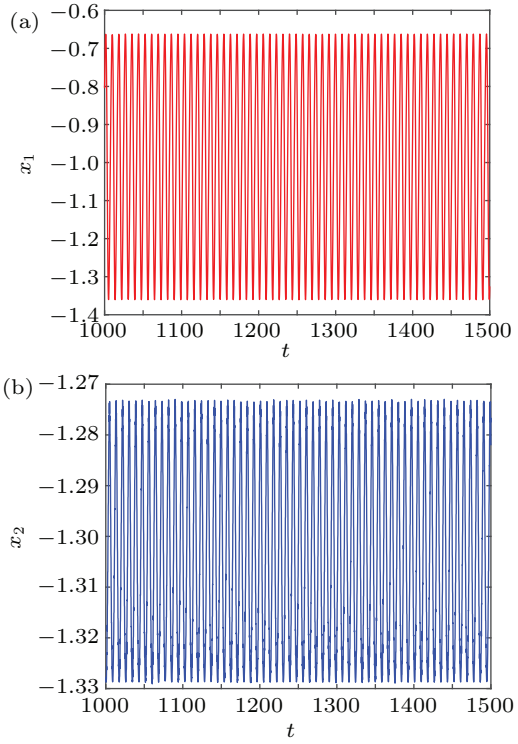


Fig. 11. The time series of membrane potentials. (a) FHN neuron, (b) HR neuron. The coupling strength $k = 1$, the initial value is ($x_1 = -1$, $y_1 = -0.8$, $x_2 = -1.36$, $y_2 = -8$, $\phi = 0.065$), and the time delay $\tau_1 = \tau_2 = 2.2$. Both neurons exhibit periodic firing due to the time delays are greater than $\tau^0 = 2.036$.

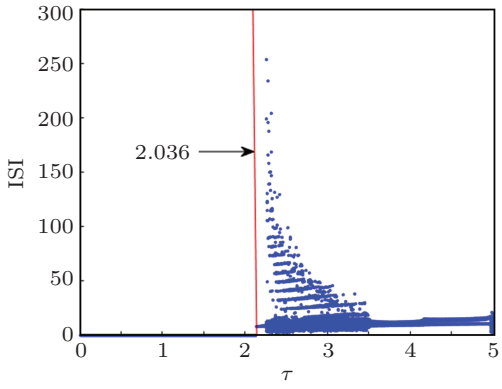


Fig. 12. The ISI bifurcation diagram of membrane potential x_1 for FHN neuron respect to the time delay $\tau = \tau_1 = \tau_2$ with the coupling strength $k = 1$ and the initial value ($x_1 = -1$, $y_1 = -0.8$, $x_2 = -1.36$, $y_2 = -8$, $\phi = 0.065$).

Case 4 $\tau_1 > 0$, $\tau_2 > 0$, $\tau_1 \neq \tau_2$. Let $\lambda = \mathrm{i}\omega$ be the root of characteristic equation (6) and get

$$\begin{aligned}&\mathrm{i}\omega^5 + B_1\omega^4 - B_2\omega^3\mathrm{i} - B_3\omega^2 + B_4\omega\mathrm{i} + B_5\\&+(C_1\omega^4 - C_2\omega^3\mathrm{i} - C_3\omega^2 + C_4\omega\mathrm{i} + C_5)\\&\times[\cos(\omega\tau_1) - \mathrm{i}\sin(\omega\tau_1)]\\&+(D_1\omega^4 - D_2\omega^3\mathrm{i} - D_3\omega^2 + D_4\omega\mathrm{i} + D_5)\\&\times[\cos(\omega\tau_2) - \mathrm{i}\sin(\omega\tau_2)] = 0. \end{aligned} \quad (23)$$

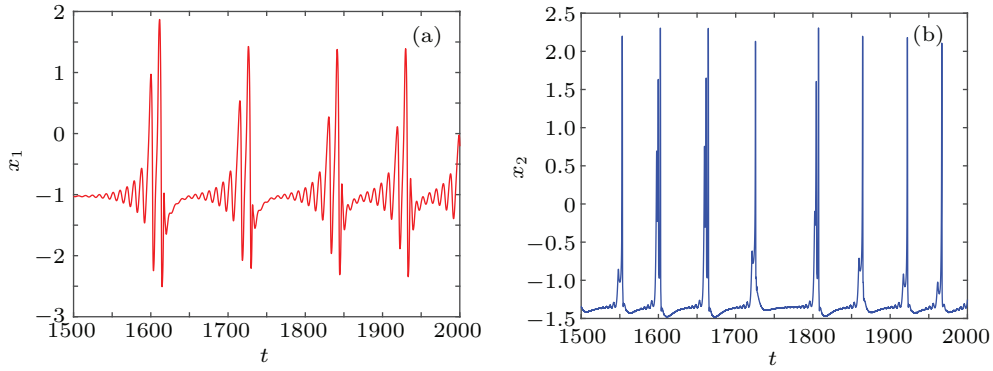


Fig. 13. The time series of membrane potentials. (a) FHN neuron, (b) HR neuron. The coupling strength $k = 1$, the initial value is ($x_1 = -1$, $y_1 = -0.8$, $x_2 = -1.36$, $y_2 = -8$, $\phi = 0.065$), and the time delay $\tau_1 = \tau_2 = 2.5$. Chaotic firing emerges in two neurons.

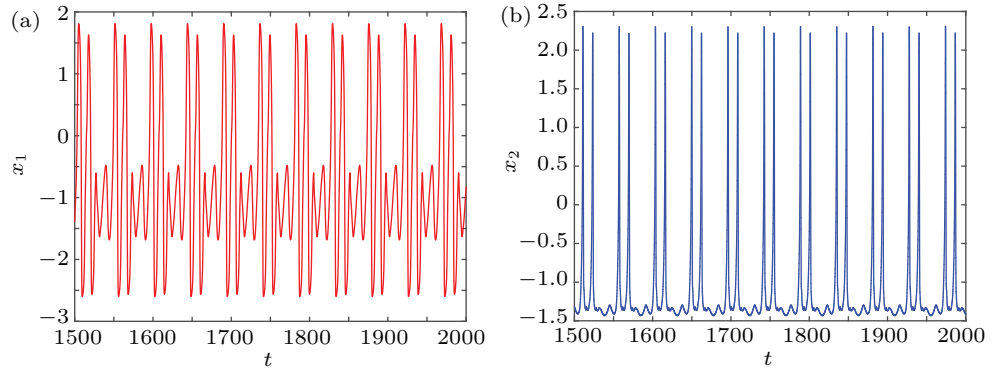


Fig. 14. The time series of membrane potential. (a) FHN neuron, (b) HR neuron. The coupling strength $k = 1$, the initial value is ($x_1 = -1$, $y_1 = -0.8$, $x_2 = -1.36$, $y_2 = -8$, $\phi = 0.065$), and the time delay $\tau_1 = \tau_2 = 4$. Periodic firing are observed in two neurons.

Without loss of generality, we suppose τ_2 is in its stable interval, *i.e.*, $\tau_2 \in [0, \tau_2^0]$, and regard $\tau_1$as a controlling parameter. Separating the real and imaginary part of Eq. (23), we get

$$\begin{cases} A_1 + m\cos(\omega\tau) + n\sin(\omega\tau) = 0, \\ A_2 - m\sin(\omega\tau) + n\cos(\omega\tau) = 0, \end{cases} \tag{24}$$

where

$$\begin{aligned} A_1 &= B_1\omega^4 - B_3\omega^2 + B_5 + (D_1\omega^4 - D_3\omega^2 + D_5) \\ &\quad \times \cos(\omega\tau_2) + (D_4\omega - D_2\omega^3)\sin(\omega\tau_2), \\ A_2 &= \omega^5 - B_2\omega^3 + B_4\omega - (D_1\omega^4 - D_3\omega^2 + D_5) \\ &\quad \times \sin(\omega\tau_2) + (D_4\omega - D_2\omega^3)\cos(\omega\tau_2), \\ m &= C_1\omega^4 - C_3\omega^2 + C_5, \\ n &= C_4\omega - C_2\omega^3, \end{aligned} \tag{25}$$

which leads to

$$\begin{aligned} &\omega_{10} + e_1\omega^9 + e_2\omega^8 + e_3\omega^7 + e_4\omega^6 + e_5\omega^5 \\ &+ e_6\omega^4 + e_7\omega^3 + e_8\omega^2 + e_9\omega + e_{10} = 0, \end{aligned} \tag{26}$$

where

$$\begin{aligned} e_1 &= -2D_1\sin(\omega\tau_2), \\ e_2 &= D_1^2\sin^2(\omega\tau_2) - 2B_2 - 2D_2\cos(\omega\tau_2) + [B_1 + D_1\cos(\omega\tau_2)]^2 - C_1^2, \\ e_3 &= 2D_3\sin(\omega\tau_2) - 2D_2\sin(\omega\tau_2)[B_1 + D_1\cos(\omega\tau_2)] + 2D_1\sin(\omega\tau_2)[B_2 + D_2\cos(\omega\tau_2)], \\ e_4 &= 2B_4 + 2C_1C_3 + D_2^2\sin^2(\omega\tau_2) + 2D_4\cos(\omega\tau_2) + [B_2 + D_2\cos(\omega\tau_2)]^2 - C_2^2 \\ &\quad - 2[B_1 + D_1\cos(\omega\tau_2)][B_3 + D_3\cos(\omega\tau_2)] - 2D_1D_3\sin^2(\omega\tau_2), \\ e_5 &= 2D_4\sin(\omega\tau_2)[B_1 + D_1\cos(\omega\tau_2)] - 2D_5\sin(\omega\tau_2) - 2D_3\sin(\omega\tau_2)[B_2 + D_2\cos(\omega\tau_2)] \\ &\quad + 2D_2\sin(\omega\tau_2)[B_3 + D_3\cos(\omega\tau_2)] - 2D_1\sin(\omega\tau_2)[B_4 + D_4\cos(\omega\tau_2)], \\ e_6 &= 2C_2C_4 - 2C_1C_5 + D_3^2\sin^2(\omega\tau_2) + [B_3 + D_3\cos(\omega\tau_2)]^2 - C_3^2 + 2[B_1 + D_1\cos(\omega\tau_2)][B_5 + D_5\cos(\omega\tau_2)] \\ &\quad - 2[B_2 + D_2\cos(\omega\tau_2)][B_4 + D_4\cos(\omega\tau_2)] + 2D_1D_5\sin^2(\omega\tau_2) - 2D_2D_4\sin^2(\omega\tau_2), \\ e_7 &= 2D_5\sin(\omega\tau_2)[B_2 + D_2\cos(\omega\tau_2)] - 2D_4\sin(\omega\tau_2)[B_3 + D_3\cos(\omega\tau_2)] \\ &\quad + 2D_3\sin(\omega\tau_2)[B_4 + D_4\cos(\omega\tau_2)] - 2D_2\sin(\omega\tau_2)[B_5 + D_5\cos(\omega\tau_2)], \end{aligned}$$

$$
\begin{aligned}
e_8 &= 2C_3C_5 + D_4^2\sin^2(\omega\tau_2) + [B_4 + D_4\cos(\omega\tau_2)]^2 - C_4^2 - 2[B_3 + D_3\cos(\omega\tau_2)][B_5 + D_5\cos(\omega\tau_2)] - 2D_3D_5\sin^2(\omega\tau_2),\\
e_9 &= 2D_4\sin(\omega\tau_2)[B_5 + D_5\cos(\omega\tau_2)] - 2D_5\sin(\omega\tau_2)[B_4 + D_4\cos(\omega\tau_2)],\\
e_{10} &= D_5^2\sin^2(\omega\tau_2) + [B_5 + D_5\cos(\omega\tau_2)]^2 - C_5^2.
\end{aligned}
$$

Taking $\tau_2 = 2$ in the stable interval of τ_2, and substituting equilibrium point E_1 into Eq. (26), two roots $\omega_1 = 0.13$ and $\omega_2 = 0.77$ are obtained, corresponding to $\tau_1^{(j)} = -10.8 + 48.33j$ and $\tau_2^{(j)} = 2.15 + 8.16j$. Finally, we can get the Hopf bifurcation point $\tau_1^0 = 2.15$ when $\tau_2 = 2$.

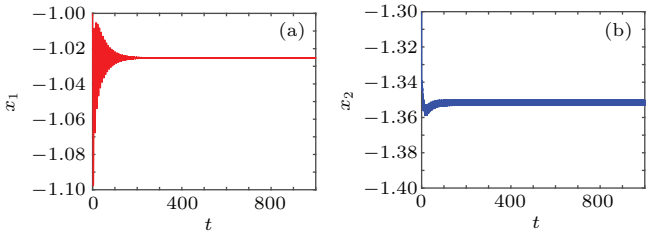


Fig. 15. The time series of membrane potential: (a) FHN neuron, (b) HR neuron. The coupling strength $k = 1$, the initial value is ($x_1 = -1$, $y_1 = -0.8$, $x_2 = -1.3$, $y_2 = -8$, $\phi = 0.065$), and the time delay $\tau_1 = 2$, $\tau_2 = 2$. Both neurons are quiescent due to the time delay τ_1 is less than $\tau_1^0 = 2.15$.

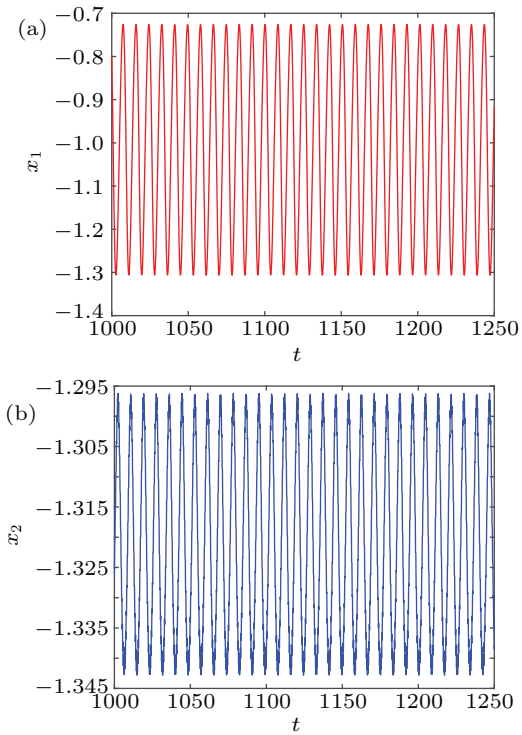


Fig. 16. The time series of membrane potentials corresponding to different neurons. (a) FHN neuron, (b) HR neuron, where the coupling strength $k = 1$, the initial value is ($x_1 = -1$, $y_1 = -0.8$, $x_2 = -1.3$, $y_2 = -8$, $\phi = 0.065$), and the time delay $\tau_1 = 2.2$, $\tau_2 = 2$. Both neurons exhibit periodic firing due to the time delay τ_1 is greater than $\tau_1^0 = 2.15$.

Through the above analysis, we know that the network is local asymptotically stable when $\tau_2 = 2$ and, $\tau_1 = 2 < \tau_1^0 = 2.15$, as illustrated in Fig. 15. And when τ_1 surpasses the critical value τ_1^0, a family of periodic solutions bifurcate from E_1, as shown in Fig. 16. Without losing generality, the two parameters bifurcation diagram of τ_1 and τ_2 is shown in Fig. 17.

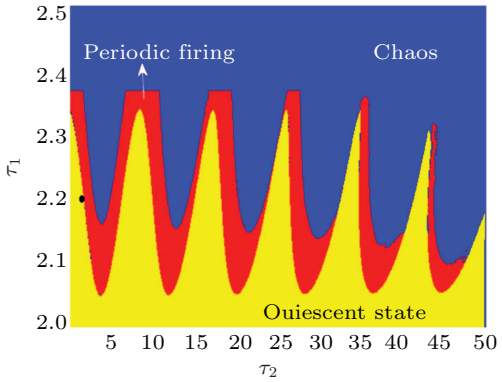


Fig. 17. Two parameters bifurcation diagram of τ_1 and τ_2, where the coupling strength $k = 1$, the initial value is ($x_1 = -1$, $y_1 = -0.8$, $x_2 = -1.3$, $y_2 = -8$, $\phi = 0.065$). The yellow, red, and blue regions represent quiescent state, periodic firing, and chaos, respectively, and the black dot is the Hopf bifurcation point.

4. Phase synchronization of two time delays neuron network

Synchronous behavior has always been a hot issue in coupled neural networks, numerous studies have shown that increasing the coupling intensity can effectively promote synchronization between neurons. However, the existing studies have mainly focused on the synchronization between the same neurons. Studying the synchronization between heterogeneous neurons can help us reveal how neurons with significantly different intrinsic dynamics affect each other's firing activities. Additionally, the effect of time-delay on the phase synchronization in memristor-coupled systems is rarely studied. Therefore, this section will reveal how time delay affects the synchronous firing behavior between different neurons.

First of all, the phase $\theta(t)$ of a periodic or chaotic motion can be calculated by the following equation:

$$\theta(t) = 2\pi n + 2\pi\frac{t - t_n}{t_{n+1} - t_n}, \quad (t_n < t < t_{n+1}), \tag{27}$$

where t_n is the time when the n-th burst appears. It can be seen from this expression that the phase increases with the increase of discharge times, each time the neuron releases an action potential, its phase increases by 2π. Hence, the phase synchronization of two neurons can be identified by detecting whether the absolute value of the phase difference $|\Delta\theta(t)| = |\theta_1(t) - \theta_2(t)|$ is bounded with the value of 2π.

There are two time delays in our system. We will discuss the effects of the two delays on the synchronization behavior of the system, separately. When fixed the coupling strength $k = 10$ and the time delay $\tau_1 = 0$, the time series of membrane potentials and the corresponding phase differences with $\tau_2 = 0$, 0.1, 1, and 10 are illustrated in Fig. 18. From

Fig. 18, one can find that the firing pattern of neurons transform from 2-period bursting to chaotic bursting to 2-period bursting. Besides, with the introduction of τ_2, the phase difference changes from small fluctuation around zero to large spike fluctuation, and finally to a mountain-like jump, indicating that the time delay τ_2 will hinder the synchronization between neurons. Then, let $\tau_2 = 0$, the transition of phase synchronization with $k = 10$ corresponding to different τ_1 is shown in Fig. 19. When $\tau_1 = 0.1$, both neurons exhibit 2-period bursting, and the phase difference fluctuates with a small amplitude around zero, that is to say, the two neurons are in phase synchronization. In Fig. 19(c1), one can find that mixed-mode oscillations emerge in both neurons, and the phase difference shows a spike near 10 beyond the range of $[0, 2\pi]$ as shown in Fig. 19(c2). For the larger τ_1, both neurons exhibit periodic spiking as shown in Fig. 19(d1), and the absolute value of the phase differences waves around a value greater than 2π is illustrated in Fig. 19(d2). Thus, we can conclude that the time delay τ_2 has greater effect on the desynchronization than τ_1 for the reason that the phase difference has a step jump with the increase of τ_2, while the phase difference will only oscillate slightly around a fixed value with the introduction of τ_1. This may provide some insights for studying the synchronous behavior of neural networks with multiple delays.

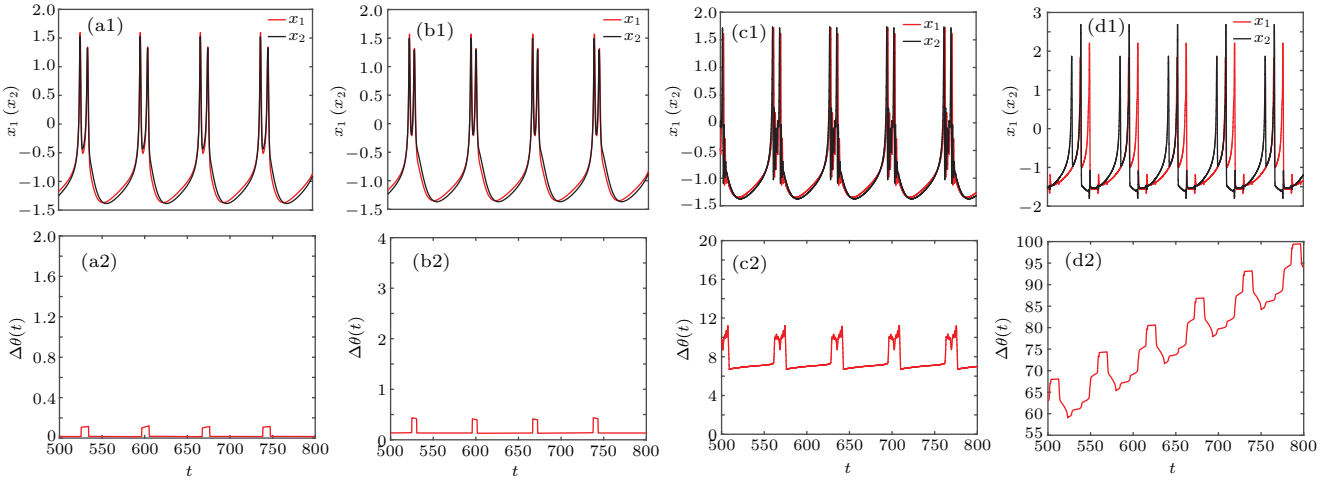


Fig. 18. The transition of phase synchronization of the memristor synapse-coupled neurons for (a) $\tau_2 = 0$, (b) $\tau_2 = 0.1$, (c) $\tau_2 = 1$, and (d) $\tau_2 = 10$, where panels (a1), (b1), (c1), and (d1) are time sequences of membrane potentials, panels (a2), (b2), (c2), and (d2) denote the phase difference of two neurons. The initial values are $(x_1 = -1, y_1 = -1.01, x_2 = -1.36, y_2 = -8, \phi = 0.065)$ and $k = 10$.

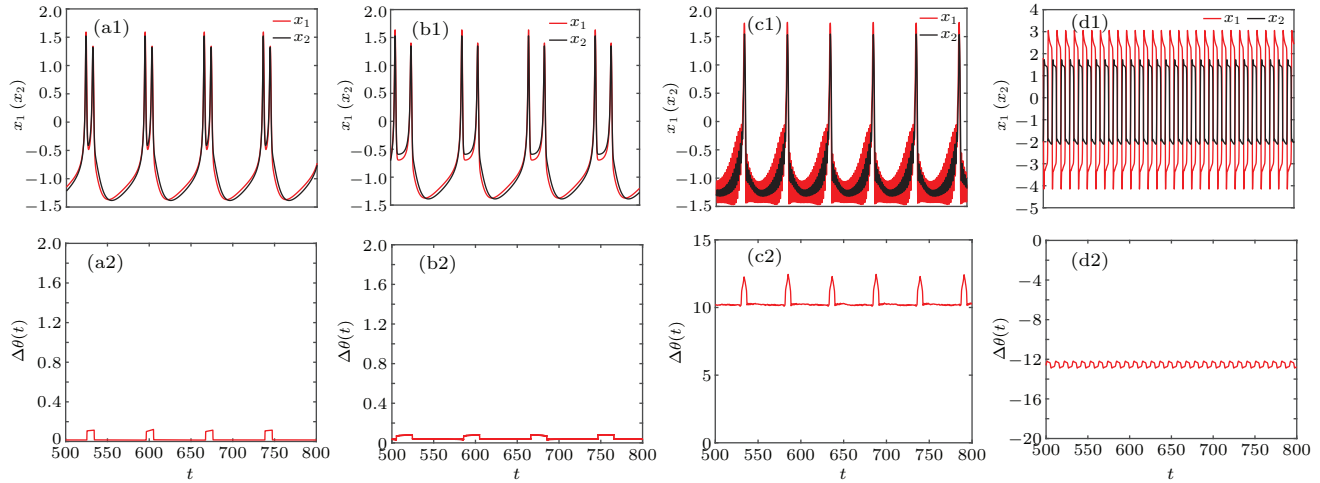


Fig. 19. The transition of phase synchronization of the memristor synapse-coupled neurons for (a) $\tau_1 = 0$, (b) $\tau_1 = 0.1$, (c) $\tau_1 = 1$, and (d) $\tau_1 = 10$, where panels (a1), (b1), (c1), and (d1) are time sequences of membrane potentials, panels (a2), (b2), (c2), and (d2) denote the phase difference of two neurons and initial values $(x_1 = -1, y_1 = -1.05, x_2 = -1.36, y_2 = -8, \phi = 0.065)$.

5. Circuit simulations

5.1. Schematics and circuit parameter selections

In this section, the memristor coupled neuron network governed by system (3) is realized by using off-the-shelf circuit components, as shown in Fig. 20, in which four crucial bipolar transistors MPS2222 and two additional operational amplifiers compose a differential amplifier to realize the hyperbolic tangent function;[50–55] the time delay function is realized by the embedded delay module in Multisim software; the operational amplifiers TL082CD and the analog multipliers AD633AN are biased with ±15 V. According to Kirch-

hoff's laws, the obtained circuit equations can be written as

$$\begin{cases} R_0C_0\dfrac{\mathrm{d}V_{x_1}}{\mathrm{d}t} = \dfrac{R_0}{R_1}V_{x_1} - \dfrac{R_0g_1g_2}{R_2}V_{x_1}^3 - \dfrac{R_0}{R_3}V_{y_1} \\ \qquad\qquad - \dfrac{R_0g_3}{R_4}[0.5+\tanh(V_\phi)](V_{x_1\tau}-V_{x_2\tau}), \\ R_0C_0\dfrac{\mathrm{d}V_{y_1}}{\mathrm{d}t} = \dfrac{R_0}{R_5}V_{x_1} + \dfrac{R_0}{R_6}V_1 - \dfrac{R_0}{R_7}V_{y_1}, \\ R_0C_0\dfrac{\mathrm{d}V_{x_2}}{\mathrm{d}t} = \dfrac{R_0}{R_8}V_{y_2} - \dfrac{R_0g_4g_5}{R_9}V_{x_2}^3 + \dfrac{R_0g_4}{R_{10}}V_{x_2}^2 \\ \qquad\qquad + \dfrac{R_0g_3}{R_4}[0.5+\tanh(V_\phi)](V_{x_1\tau}-V_{x_2\tau}), \\ R_0C_0\dfrac{\mathrm{d}V_{y_2}}{\mathrm{d}t} = \dfrac{R_0}{R_{11}}V_2 - \dfrac{R_0g_6}{R_{12}}V_{x_2}^2 - \dfrac{R_0}{R_{13}}V_{y_2}, \\ R_0C_0\dfrac{\mathrm{d}V_\phi}{\mathrm{d}t} = -\dfrac{R_0}{R_{14}}V_\phi + \dfrac{R_0}{R_{15}}(V_{x_1\tau}-V_{x_2\tau}), \end{cases} \tag{28}$$

where state variables V_{x1}, V_{y1}, V_{x2}, V_{y2}, and V_ϕ denote capacitor voltages of five integral circuit channels, respectively. Comparing Eq. (28) with Eq. (3), it is easy to find that they have same mathematical expressions. The circuit equations (28), thus, can successfully simulate firing patterns of the presented neuron model governed by Eq. (3) when the circuit parameters and the system parameters are satisfied with the following relations:

$$\begin{aligned} &R_1 = R_0, \quad R_2 = 3R_0g_1g_2, \quad R_3 = R_0, \quad R_4 = R_0g_3/k, \\ &R_5 = 10R_0, \quad R_6 = 50R_0/3, \quad R_7 = 20R_0, \\ &R_8 = R_0, \quad R_9 = R_0g_4g_5, \quad R_{10} = R_0g_4/3, \quad R_{11} = R_0, \\ &R_{12} = R_0g_6/5, \quad R_{13} = R_0, \quad R_{14} = R_0, \quad R_{15} = 5R_0. \end{aligned}$$

Based on the system parameters given in Eq. (3), assuming the integration time constant $R_0C_0 = 1000$ ms and letting $C_1 = C_2 = C_3 = C_4 = C_5 = 100$ nF, the corresponding circuit parameters can be easily determined, as shown in Table 2. It is worth noting that the multiplier output gains are determined as $g_1 = g_3 = g_4 = g_6 = 1$ and $g_2 = g_5 = 0.1$.

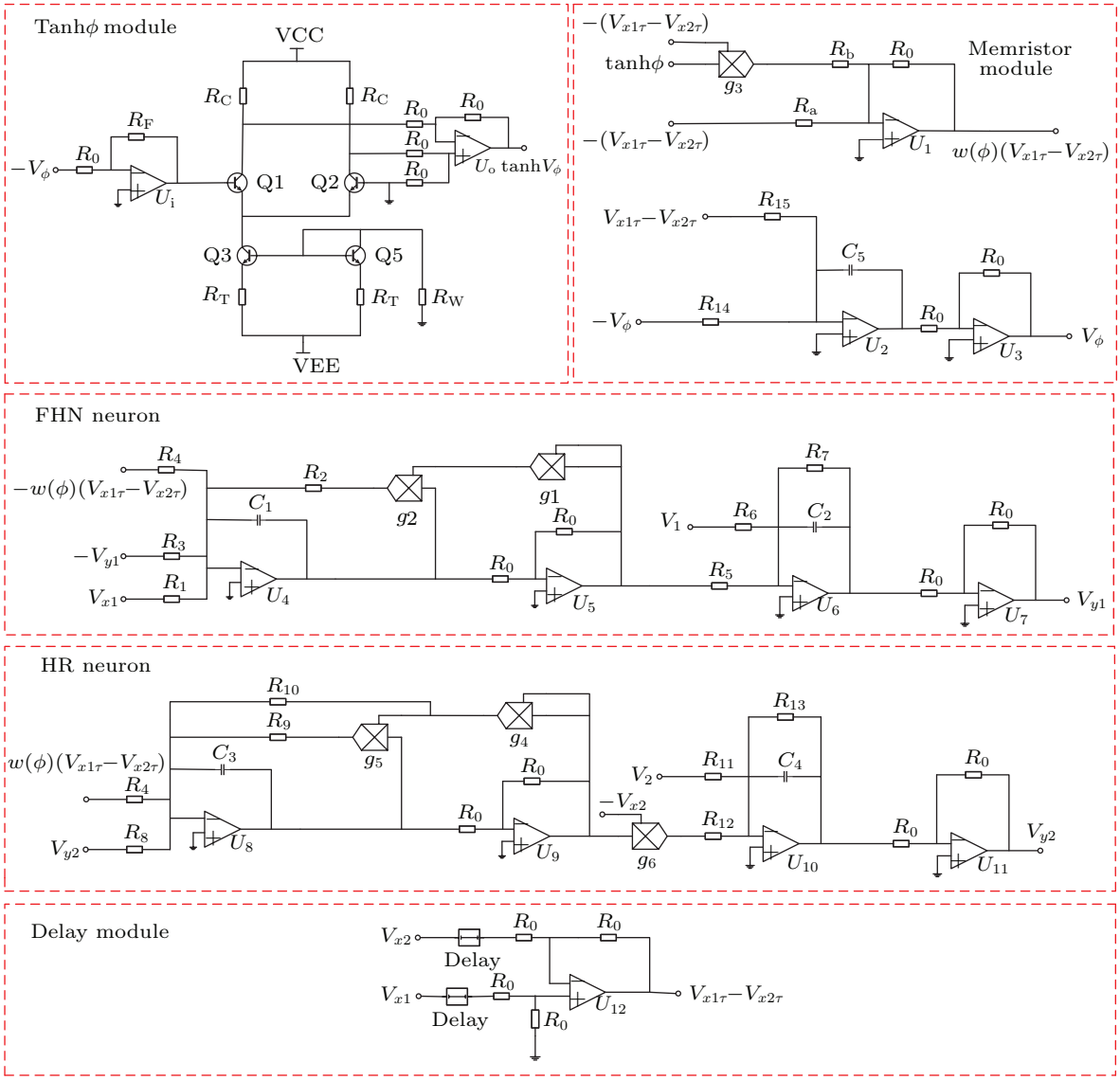


Fig. 20. Main circuit of the memristor coupling heterogeneous neurons, which contains memristor module, tanh ϕ module, time delay module, FHN and HR neurons.

Table 2. Circuit parameters of the proposed neuron circuit.

Parameters	Significations	Values
$R_0, R_1, R_3, R_8, R_{11}$	resistance	10 kΩ
R_2,	resistance	3 kΩ
R_5	resistance	100 kΩ
R_6	resistance	166.6667 kΩ
R_7	resistance	200 kΩ
R_9, R_C	resistance	1 kΩ
R_1	resistance	3.3333 kΩ
R_{12}, R_T	resistance	2 kΩ
R_{15}	resistance	50 kΩ
R_{13}, R_{14}, R_b	resistance	10 kΩ
R_F	resistance	575.5 Ω
R_W	resistance	11 kΩ
R_a	resistance	20 kΩ
VCC	DC power	15 V
VEE	DC power	−15 V
C_1, C_2, C_3, C_4, C_5	capacitance	100 nF
V_1, V_2	DC power	1 V
R_4	resistance	adjustable

5.2. Circuit simulation results

On the basis of schematics given in Fig. 20, Multisim 14.0 software is applied to simulate the proposed memristor synapse-coupled neural network with two time delays. The circuit parameters listed in Table 2 are utilized, and the initial voltages of five capacitances are same with the corresponding initial values in numerical simulations. It is noteworthy that R_4 is an adjustable resistor, which can control the coupling strength of the system.

When $\tau_1 = \tau_2 = 2.5$ ms and $R_4 = 10$ kΩ (corresponding to $k = 1$), the time series of the membrane potential x_1 and x_2 with the initial values (−1 V, −1.05 V, −1.3 V, −8 V, 0.065 V) are shown in Fig. 21. For $\tau_2 = 2$ ms, the time series of V_{x1} and V_{x2} corresponding to $\tau_1 = 2$ and 2.2 ms are plotted in Figs. 22 and 23, respectively. The Hopf bifurcation conditions, thus, obtained by theoretical analysis are further verified. Besides, when $R_4 = 1$ kΩ (corresponding to $k = 10$), the phase synchronization results with respect to different time delays are shown in Figs. 24 and 25, which confirms that the time delay impedes the phase synchronization between neurons. Ignoring some tiny differences caused by computational errors, the circuit simulation results in Figs. 21–25 are well consistent with the numerical results in Figs. 13, 15, 16, 18, and 19.

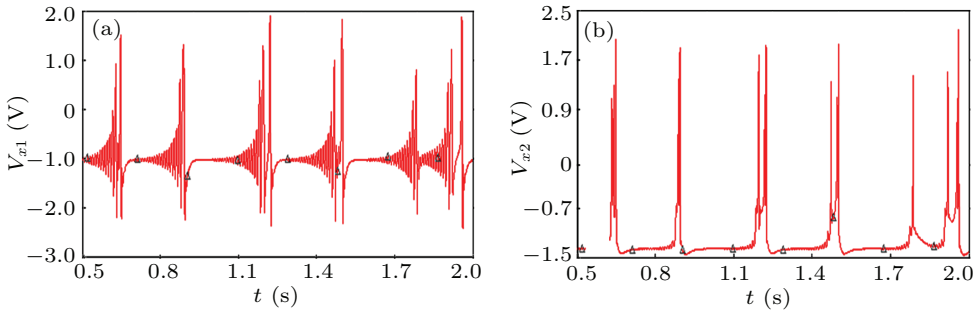


Fig. 21. Circuit simulation results for different neurons, where $\tau_1 = \tau_2 = 2.5$ ms. (a) FHN neuron, (b) HR neuron.

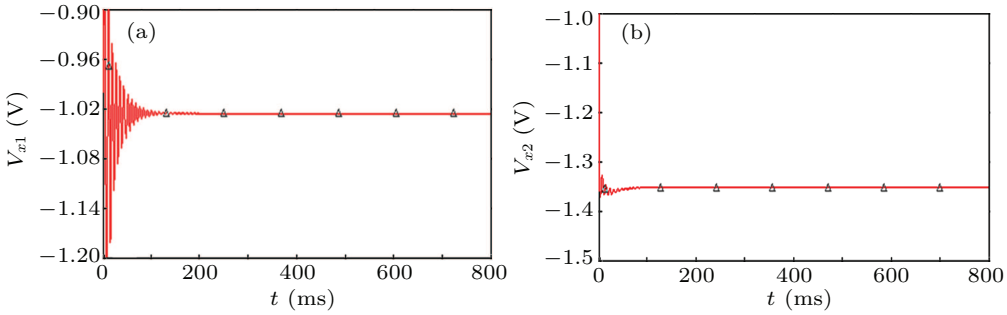


Fig. 22. Circuit simulation results with different neurons, where $\tau_1 = 2$ ms and $\tau_2 = 2$ ms. (a) FHN neuron, (b) HR neuron.

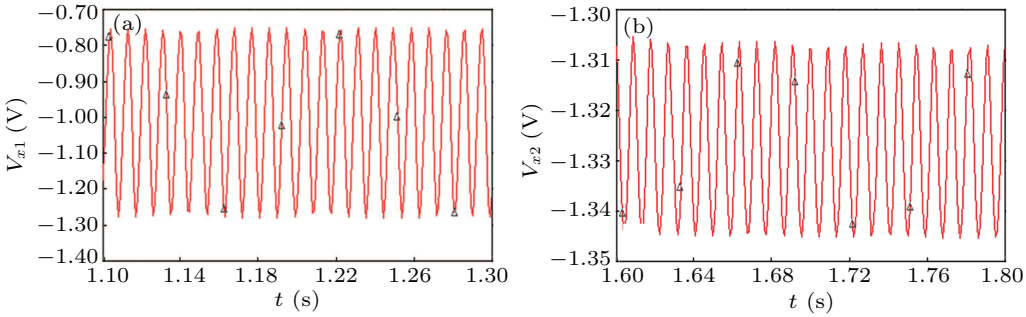


Fig. 23. Circuit simulation results with different neurons, where $\tau_1 = 2.2$ ms and $\tau_2 = 2$ ms. (a) FHN neuron, (b) HR neuron.

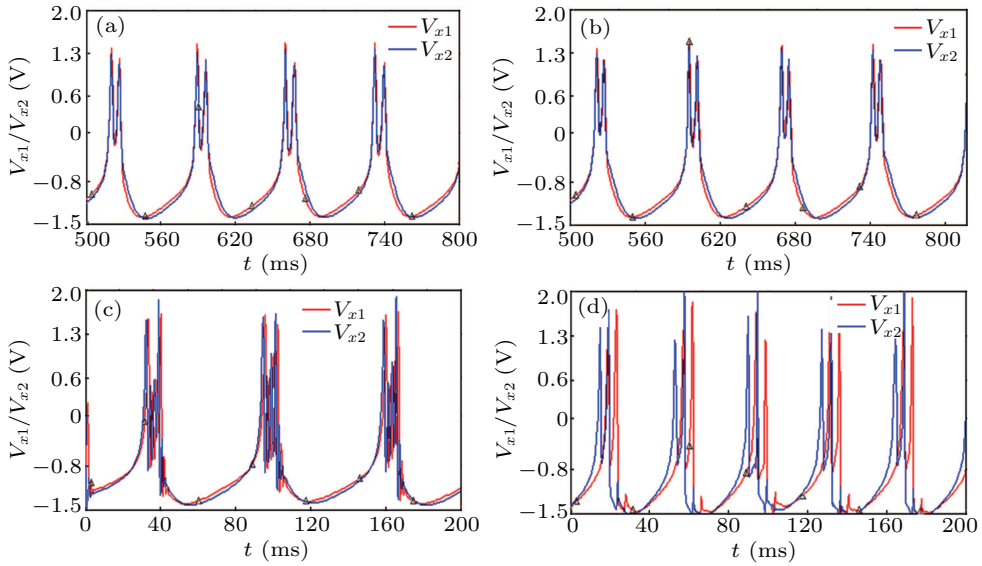


Fig. 24. Evolution of phase synchronization for (a) $\tau_2 = 0$ ms, (b) $\tau_2 = 0.1$ ms, (c) $\tau_2 = 1$ ms, and (d) $\tau_2 = 10$ ms, where $\tau_1 = 0$ ms, $R_4 = 1$ kΩ and initials (−1 V, −1.01 V, −1.36 V, −8 V, 0.065 V).

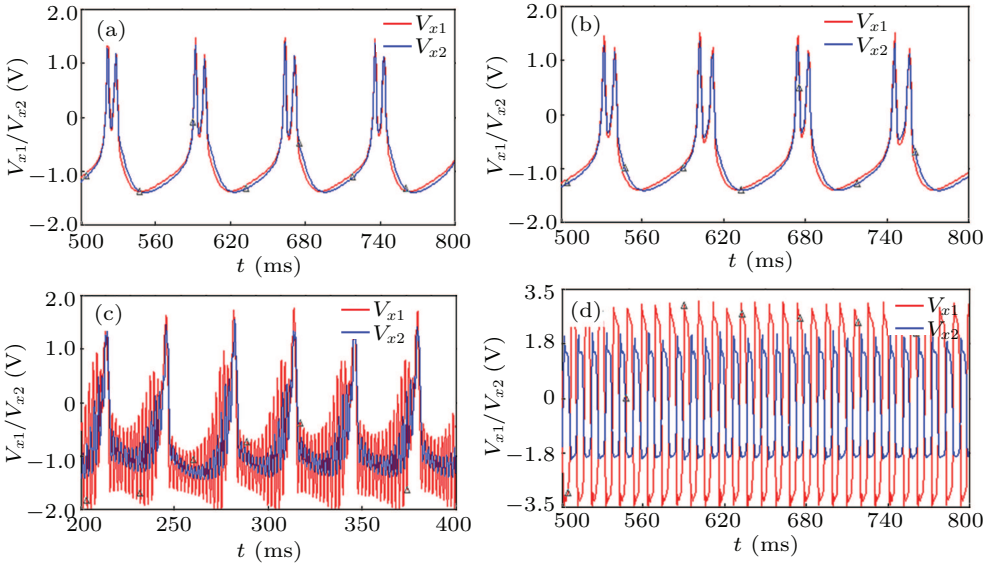


Fig. 25. Evolution of phase synchronization for (a) $\tau_1 = 0$ ms, (b) $\tau_1 = 0.1$ ms, (c) $\tau_1 = 1$ ms, and (d) $\tau_1 = 10$ ms, where $\tau_2 = 0$ ms, $R_4 = 1$ kΩ, and initials (−1 V, −1.05 V, −1.36 V, −8 V, 0.065 V).

6. Conclusions

In this work, a novel neural network is established by coupling 2D FHN and HR neurons bidirectionally with a threshold memristor, and the time delays of neural signal transmission in FHN and HR neurons are taken into account. By systematically analyzing the equilibrium stability of the proposed system, the existence of local Hopf bifurcation in four cases is obtained theoretically. Numerical simulation results show the time delays in FHN and HR neurons have different effect on firing activities of the memristor-coupled neural system. The time delay τ_2 is not sensitive due to its big critical value and can only ignite the transition from quiescent state to periodic oscillations when $\tau_1 = 0$ and $\tau_2 > 0$ (Case 1). However, the neural network is much more sensitive to τ_1 which can induce multiple firing patterns, such as quiescent state, periodic firing and chaotic firing when $\tau_1 > 0$ and $\tau_2 = 0$ (Case 2). Besides, in order to observe the influence of the two time delays on the firing behavior more intuitively, a bi-parameter bifurcation diagram for τ_1 and τ_2 is drawn. Moreover, by adjusting the time delays τ_1 and τ_2, phase synchronization between two different neurons is explored. We find that the two time delays τ_1 and τ_2 can impede the synchronous behavior between different neurons, especially, the time delay τ_2 has a greater effect on the desynchronization than the time delay τ_1. Finally, the memristor-coupled neural network is implemented with off-the-shelf circuit components, and Multisim simulation results are provided to verify the theoretical analysis. Consequently, the study may provide some insights for studying memristor-coupled neural networks with multiple delays.

Data availability

The datasets generated during and/or analyzed during the current study are available from the corresponding author on reasonable request.

Acknowledgement

Project supported by the National Natural Science Foundations of China (Grant Nos. 62171401 and 62071411).

References

[1] Yao Y, Yang L, Wang C and Liu Q 2018 *Complexity* **10** 5632650
[2] Yao Y and Ma J 2018 *Cognitive Neurodynamics* **12** 343
[3] Wu F, Ma J and Zhang G 2019 *Applied Mathematic and Computation* **347** 590
[4] Hindmarsh J L and Rose R M 1982 *Nature* **296** 162
[5] Hindmarsh J L and Rose R M 1984 *Proc. Roy. Soc. Lond. Ser. B Biolog. Sci.* **221** 87
[6] Wang H, Lu Q and Wang Q 2008 *Commun. Nonlinear Sci. Numeri. Simul.* **13** 1668
[7] Bao B, Yang Q, Zhu L and Bao H 2019 *Int. J. Bifur. Chaos* **29** 1950134
[8] Ge P and Cao H 2021 *Int. J. Bifur. Chaos* **31** 2150233
[9] Ma J, Yang Z Q, Yang L J and Tang J 2019 *Journal of Zhejiang University-Science A* **20** 639
[10] Vaidyanathan S 2015 *International Journal of PharmTech Research* **8** 117
[11] An X and Qiao S 2021 *Chaos, Solitons & Fractals* **143** 110587
[12] Lv M, Wang C, Ren G, Ma J and Song X 2016 *Nonlinear Dyn.* **85** 1479
[13] Song X, Wang H and Chen Y 2019 *Nonlinear Dyn.* **96** 2341
[14] Bashkirtseva I, Nasyrova V and Ryashko L 2018 *Chaos, Solitons & Fractals* **110** 76
[15] Wu J, Xu Y and Ma J 2017 *PLoS One.* **12** e0174330
[16] Wang Y, Ma J, Xu Y, Wu F and Zhou P 2017 *Int. J. Bifur. Chaos* **27** 1750030
[17] Wu F, Wang C, Jin W and Ma J 2017 *Physica A* **469** 81
[18] Ma J and Tang J 2017 *Nonlinear Dyn.* **89** 1569
[19] Li Z and Zhou H 2021 *Electron. Lett.* **57** 715
[20] Chua L 1971 *IEEE Trans. Circuit Theory* **18** 507
[21] Ma M, Yang Y, Qiu Z, Peng Y and Sun Y 2022 *Nonlinear Dyn.* **107** 2935
[22] Wen Z, Li Z and Li X 2019 *Chaos Solitons & Fractals* **128** 58
[23] Shao N, Zhang S and Shao S 2019 *Acta Phys. Sin.* **68** 198502 (in Chinese)
[24] Zhu L and Wang F 2019 *Acta Phys. Sin.* **68** 198501 (in Chinese)
[25] Eccles J C 1982 *Ann. Rev. Neurosci.* **5** 325
[26] Zhang P, Xia M, Zhuge F, Zhou Y and Wang Z 2019 *Nano Lett.* **19** 4279
[27] Kazantsev V B and Asatryan S Y 2011 *Phys. Rev. E* **84** 031913
[28] Tan Y and Wang C 2020 *Chaos* **30** 053118
[29] Lin H, Wang C, Hong Q and Sun Y 2020 *IEEE Transacti on Circuits and Systems II: Express Briefs* **67** 3472
[30] Wu F, Zhang Y and Zhang X 2019 *Nonlinear Dyn.* **98** 971
[31] Li R, Wang Z and Dong E 2021 *Nonlinear Dyn.* **104** 4459
[32] Xu Y, Jia Y, Ma J, Alsaedi A and Ahmad B 2017 *Chaos, Solitons & Fractals* **104** 435
[33] Bao H, Zhang Y, Liu W and Bao B 2020 *Nonlinear Dyn.* **100** 937
[34] Li Z, Zhou H, Wang M and Ma M 2021 *Nonlinear Dyn.* **104** 1455
[35] Hu D and Cao H 2016 *Int. J. Bifur. Chaos.* **26** 1650187
[36] Liao X, Wong K W, Leung C S and Wu Z 2001 *Chaos, Solitons & Fractals* **12** 1535
[37] Xu Y and Ma J 2021 *Chin. Phys. B* **30** 100501
[38] Wang Z, Wang X, Li Y and Huang X 2017 *Int. J. Bifur. Chaos* **27** 1750209
[39] Wang C J, Yang K L and Qu S X 2014 *Phys. Scr.* **89** 105001
[40] Li Z, Guo Z, Wang M and Ma, M 2021 *AEU-International Journal of Electronics and Communications* **142** 153995
[41] Liu Q, Liao X, Liu Y, Zhou S and Guo S 2009 *Nonlinear Dyn.* **58** 573
[42] Liao X, Guo S and Li C 2007 *Nonlinear Dyn.* **49** 319
[43] He X, Li C, Huang T and Li C 2013 *IEEE Transactions on Neural Networks and Learning Systems* **24** 1001
[44] Zhang W, Li C, Huang T and He X 2015 *IEEE Transactions on Neural Networks and Learning Systems* **26** 3308
[45] Huang S, Zhang J, Wang M and Hu C K 2018 *Physica A* **499** 88
[46] Xiao M, Zheng W X, Jiang G and Cao J 2020 *IEEE Transactions on Neural Networks and Learning Systems* **32** 1974
[47] Li L, Zhao Z and Gu H 2019 *Int. J. Bifur. Chaos* **29** 1950147
[48] Marsden J E and McCracken M 2012 *Springer Science & Business Media* **19** 13542
[49] Walschap G 2012 *Springer Science & Business Media* **224** 116
[50] Bao H, Hu A, Liu W and Bao B 2019 *IEEE Transactions on Neural Networks and Learning Systems* **31** 502
[51] Bao B, Qian H, Xu Q, Chen M and Wang J 2017 *Frontiers in Computational Neuroscience* **11** 81
[52] Ma M, Xie X and Li Z 2023 *Chin. Phys. B* **32** 058701
[53] Ma M, Lu Y and Li Z 2023 *Fractal and Fractional.* **7** 82
[54] Ma M, Xiong K and Li Z 2023 *Mathematics* **11** 375
[55] Ma M, Yang Y and Qiu Z 2022 *Nonlinear Dyn.* **107** 2935